Chapter 5

Antibacterial efficacy

The current chapter investigates the antibacterial activity of 1- and 2-D HA nanocrystals, such as HA nanorods, nanoplates, and thin nanoplates, using E. coli and S. aureus bacteria. The antibacterial activity of various concentrations and morphologies of HA nanocrystals is evaluated using a number of quantitative and qualitative techniques. The bactericidal effect of HA nanocrystals is assessed through the quantification of ROS generation ($O_2^{-\bullet}$ and H_2O_2) within bacterial cells using SOD and catalase assays. Also, the ROS-induced damage to cellular components, like proteins and lipid membranes is evaluated utilizing Lowry protein estimation and LPO assays. In addition, the detailed mechanism behind the morphology-dependent antibacterial activity of HA nanocrystals has also been explored by considering various factors, such as concentration, size, ion release, particle agglomeration, crystallinity, and surface charge.

5.1. Antibacterial reponse

5.1.1. Quantitative assessment

5.1.1.1. Bacterial viability

Fig. 5.1A presents a comparative evaluation of the viability of *E. coli* and *S. aureus* bacteria treated with various concentrations of HA nanorods (HA5), nanoplates (HA9.5), and thin nanoplates (HA-6h). Statistical analyses show that the bacterial viability on the control sample is significantly higher than all the concentrations of different morphological HA nanocrystals, revealing the strong antibacterial potential of HA nanocrystals. However, the antibacterial effectiveness of HA nanocrystals varies depending on their morphology and concentration. For HA nanorods, 0.2 and 20 mg/ml are optimal concentrations for achieving a good antibacterial response. However, for HA nanoplates and thin nanoplates, the antibacterial response is significantly high for all the chosen concentrations (0.2, 2 and 20 mg/ml). From a

morphological perspective, HA nanorods exhibit higher antibacterial response i.e., 16.1 and 10 % reduction in bacterial viability for both types of bacteria, as compared to HA nanoplates and thin nanoplates at a sample concentration of 0.2 mg/ml. In contrast, HA thin nanoplates demonstrate greater antibacterial response than HA nanorods and nanoplates at chosen concentrations of 2 and 20 mg/ml, and the antibacterial activity of HA nanoplates lies in intermediate stage to HA nanorods and thin nanoplates for all chosen concentrations. Among all the samples, 20 mg/ml concentrated HA thin nanoplates and 0.2 mg/ml concentrated HA nanorods possess the highest and slightly lower antibacterial response for both the bacterial cells, respectively.

To further clarify the aforementioned variation in the antibacterial activity of HA nanorods, nanoplates, and thin nanoplates, their corresponding antibacterial ratio for similar bacteria is also evaluated using equation (2.2), as shown in Fig. 5.1B.

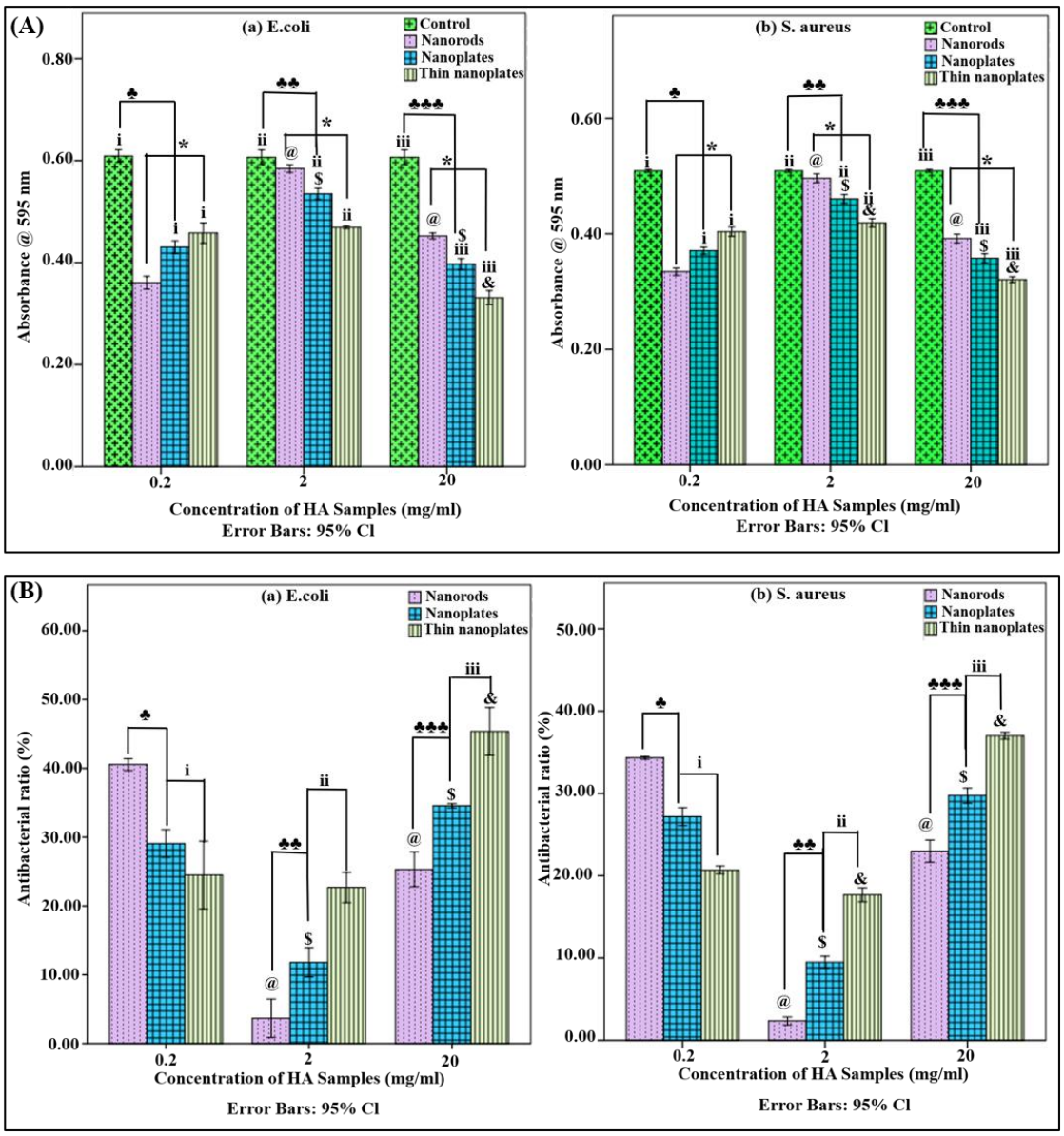

Figure 5.1. *(A) The histogram plot, representing the quantitative assessment of antibacterial response towards different concentrations of HA nanorods, nanoplates, and thin nanoplates for (a) E. coli and (b) S. aureus bacteria. (B) The corresponding antibacterial ratio for E. coli and S. aureus bacteria, treated with different concentrations of HA nanorods, nanoplates, and thin nanoplates. The mark (*) represents the significant difference in mean absorbance of all morphologies of HA nanocrystals at concentrations of 0.2, 2 and 20 mg/ml with respect to control at $p \leq 0.05$. The marks (i), (ii) and (iii) represent the significant difference in mean absorbance of HA nanoplates and thin nanoplates as well as control as compared to HA nanorods at concentrations of 0.2, 2, and 20 mg/ml at $p \leq 0.05$, respectively. The marks (♣),*

(♣♣), (♣♣♣) indicate the significant difference in mean absorbance of HA nanorods and nanoplates as well as control as compared to HA thin nanoplates at concentrations of 0.2, 2, and 20 mg/ml, at $p \leq 0.05$, respectively. The marks (@), ($) and (&) show the significant difference in mean absorbance of HA nanorods, nanoplates and thin nanoplates, respectively, among the different concentrations.

5.1.2. Qualitative assessment

5.1.2.1. Colony-counting

Fig. 5.2A (a and b) shows the outcomes of a colony counting test, used to qualitatively assess the antibacterial potential of different morphological HA nanocrystals at various concentrations (0.2, 2 and 20 mg/ml) against *E. coli* and *S. aureus* bacteria, respectively. The antibacterial effect was evaluated by counting the number of bacterial colonies (CFUs) on agar plates. Results clearly demonstrate a significant reduction in CFU formation on agar plates after exposing both the bacteria to 0.2, 2 and 20 mg/ml of concentrations of HA nanocrystals, i.e., HA nanorods, nanoplates, and thin nanoplates. Following the number of CFUs, HA nanorods, nanoplates, and thin nanoplates at a concentration of 0.2 mg/ml, show antibacterial response in descending order. In contrast, at concentrations of 2 and 20 mg/ml, the same morphologies show antibacterial activity in ascending order. Notably, at 2 mg/ml, HA nanocrystals are more prone to bacterial growth across all morphologies, with HA nanorods exhibiting the least antibacterial activity. HA thin nanoplates at 20 mg/ml demonstrate the highest antibacterial potential. A slightly poor antibacterial response is observed for HA nanorods at 0.2 mg/ml. The corresponding antibacterial ratio is also calculated using equation (2.3) which is depicted in Fig. 5.2B.

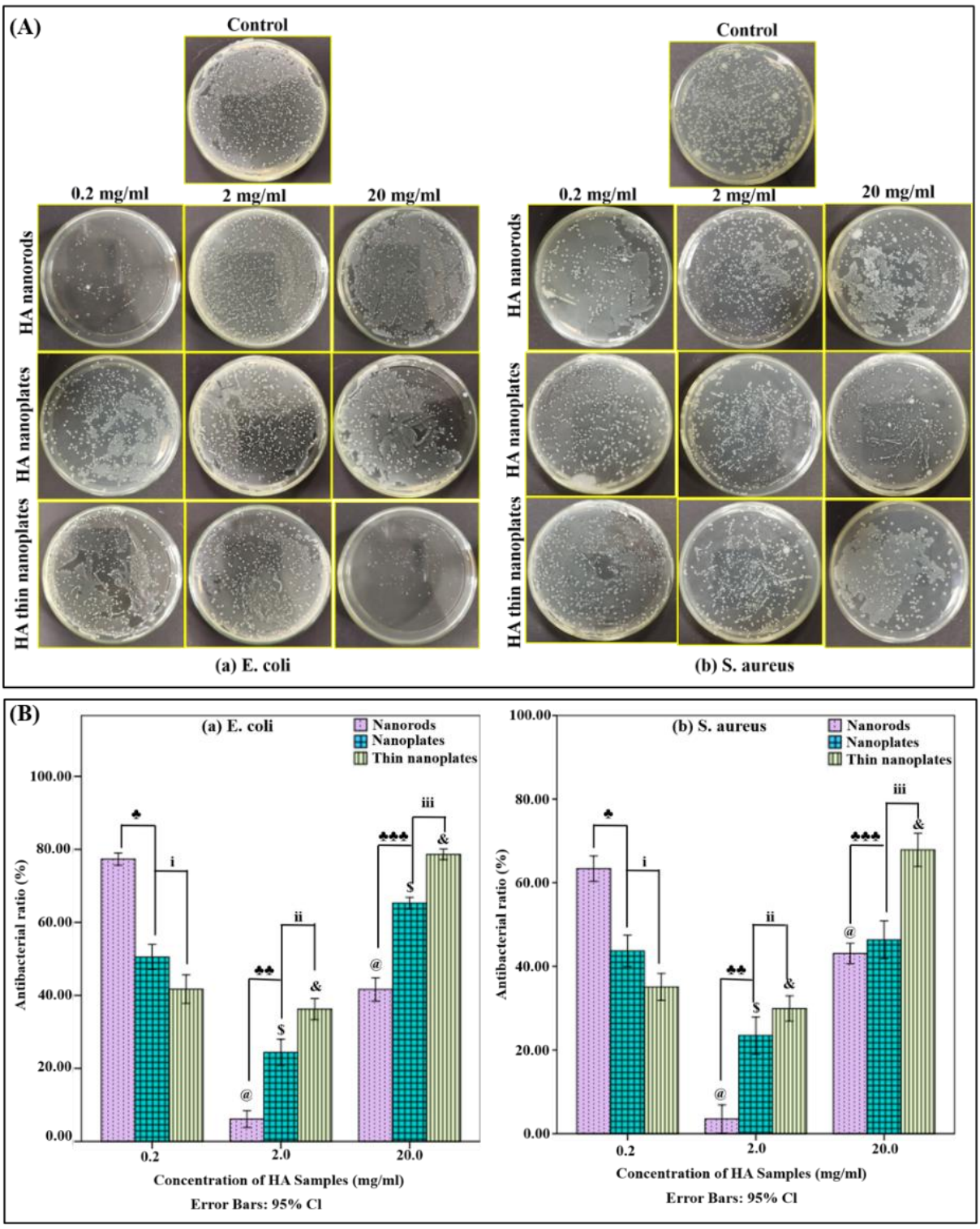

Figure 5.2. *(A) The digital images, representing the number of colonies on agar plates for E. coli and S. aureus bacteria, treated with HA nanorods, nanoplates, and thin nanoplates at various concentrations of 0.2, 2 and 20 mg/ml. (B) The antibacterial ratio of corresponding HA treated E. coli and S. aureus bacteria.*

5.1.2.2. Live-dead assay

The population of live and dead bacteria, *E. coli* and *S. aureus*, treated with different morphological HA nanocrystals, i.e., HA nanorods, nanoplates, and thin nanoplates, at various concentrations (0.2, 2 and 20 mg/ml), were assessed using fluorescence microscopy. From Fig. 5.3, it is observed that the population of dead bacteria is higher on HA nanorods than on HA nanoplates and much higher than on HA thin nanoplates for both the bacteria at a sample concentration of 0.2 mg/ml. Clearly, the antibacterial activity of HA nanorods, nanoplates, and thin nanoplates is decreasing in order for both bacteria. However, on increasing the HA concentration from 0.2 to 2 mg/ml, the density of live bacterial cells increases for all the morphologies, showing less antibacterial activity than at the concentration of 0.2 mg/ml. Also, HA nanorods, nanoplates, and thin nanoplates demonstrate antibacterial response in increasing order. On further increasing the HA concentration from 2 to 20 mg/ml, the density of live bacteria again decreases for all the respective morphologies, which is even lower than bacteria, treated with 0.2 mg/ml of HA. At 20 mg/ml concentration, thin HA nanoplates show a higher antibacterial response than HA nanorods and nanoplates. Overall, HA nanorods at a concentration of 0.2 mg/ml and thin nanoplates at a concentration of 20 mg/ml show a higher antibacterial response than other samples for both the bacteria. This result is in good agreement with MTT and colony-counting results.

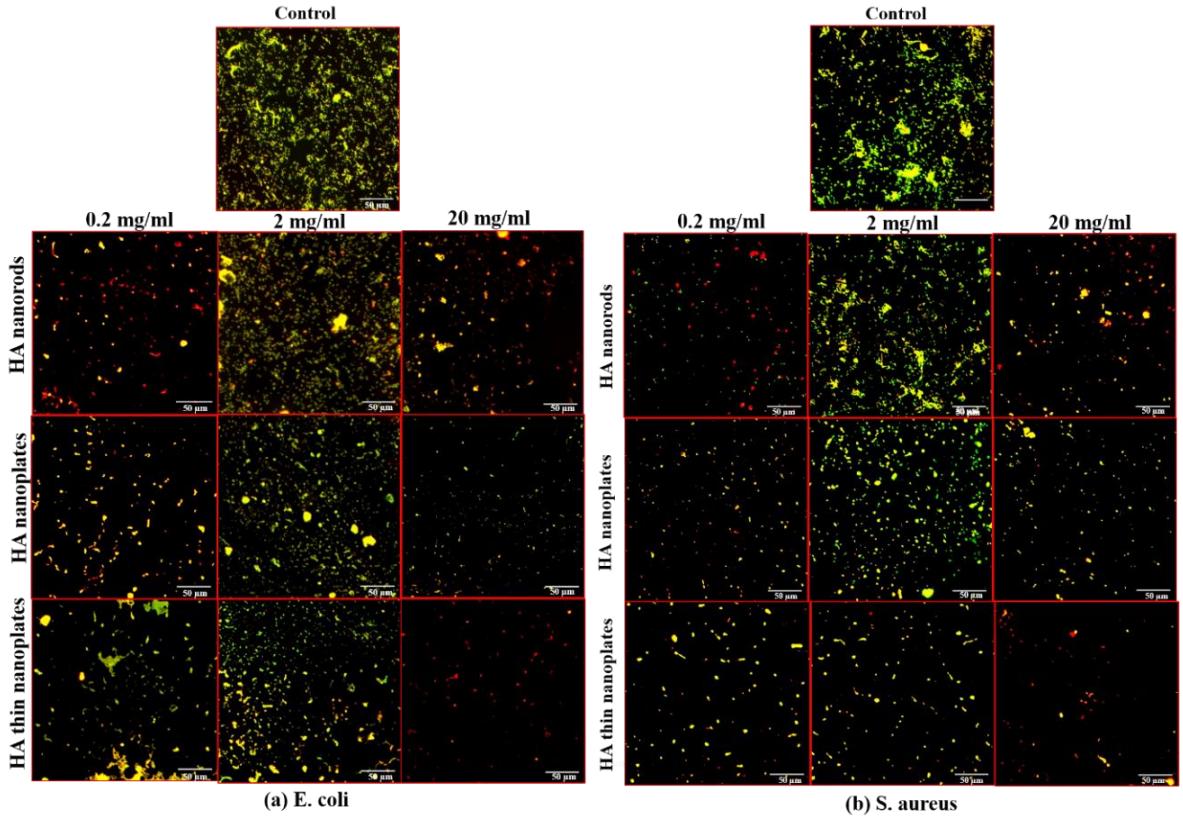

Figure 5.3. *Fluorescence microscopic images of stained live and dead bacteria, E. coli (a) and S. aureus (b), after treating with HA nanorods, nanoplates, and thin nanoplates at various concentrations of 0.2, 2 and 20 mg/ml.*

5.1.3. ROS assessment

5.1.3.1. Superoxides estimation

The production of superoxide anions ($O_2^{\bullet -}$) within *E. coli* and *S. aureus* bacterial cells, treated with various concentrations of different morphological HA nanocrystals viz. nanorods, nanoplates, and thin nanoplates was assessed using SOD assay (Fig. 5.4). The statistical analyses reveal that, at 0.2 mg/ml, HA nanorods produce considerably higher superoxides than HA nanoplates and thin nanoplates for both, *E. coli* and *S. aureus* bacteria. Increasing the concentration of HA nanocrystals from 0.2 to 2 mg/ml results in a drastic reduction in the superoxide production for similar bacteria. At this concentration, the superoxide production for both the bacteria, cultured with HA nanorods is higher than HA nanoplates and lower than HA

thin nanoplates. On further increasing the concentration of HA samples from 2 to 20 mg/ml, the number of superoxide ions for both the bacteria, again increases for all morphologies. At 20 mg/ml of HA concentration, the variation in superoxide production as per morphology is same as the variation observed at 2 mg/ml, with the highest superoxide production in HA thin nanoplates. Higher concentration of superoxide ions increases oxidative stress within bacterial cells, which disturbs the normal metabolic process of bacterial cells through oxidative damage of intracellular components that ultimately causes bacterial death [68].

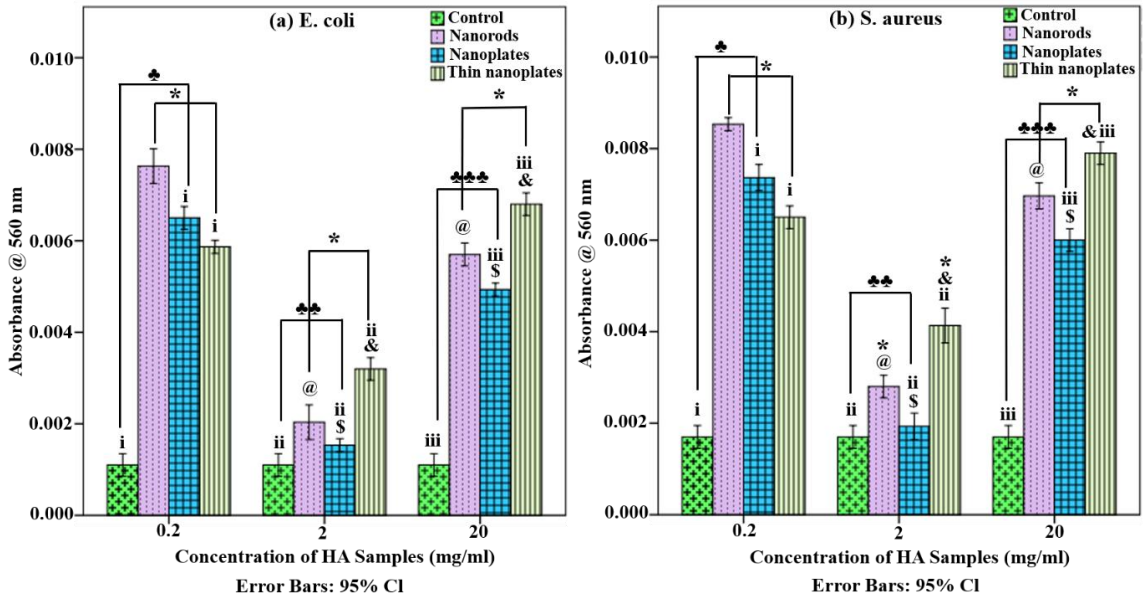

Figure 5.4. *The absorbance plot, demonstrating the concentration of superoxide anions ($O_2^{\bullet-}$) for E. coli and S. aureus bacterial cells after treating with HA nanorods, nanoplates, and thin nanoplates at various concentrations of 0.2, 2 and 20 mg/ml. The mark (*) represents the significant difference in mean absorbance for all the morphologies of HA nanocrystals at 0.2, 2 and 20 mg/ml with respect to control, at $p \leq 0.05$. The marks (i), (ii) and (iii) represent the significant difference in mean absorbance of HA nanoplates and thin nanoplates as well as control as compared to HA nanorods at concentrations of 0.2, 2, and 20 mg/ml, respectively, at $p \leq 0.05$. The marks (♣), (♣♣), (♣♣♣) indicate the significant difference in mean absorbance of HA nanorods and nanoplates as well as control as compared to HA thin nanoplates at concentrations of 0.2, 2, and 20 mg/ml, respectively, $p \leq 0.05$. The marks (@), ($) and (&)*

show the significant difference in mean absorbance of HA nanorods, nanoplates and thin nanoplates, respectively, among the different concentrations.

5.1.3.2. Evaluation of H_2O_2 dissociation

The catalase activity per sec was measured to evaluate the rate of dissociation of H_2O_2 by catalase enzyme for both, *E. coli* and *S. aureus* bacteria, after culture with various concentrations of HA nanorods, nanoplates, and thin nanoplates. Their comparative statistical analyses are depicted in Fig. 5.5. The highest catalase activity on the control surface indicates the fastest rate of H_2O_2 dissociation as compared to all the developed HA morphologies, resulting in a relatively low number of reactive H_2O_2 within both the bacterial cells, which ultimately enhances the resistance towards bacterial death. The significant reduction in catalase activity occurred on 0.2 and 20 mg/ml concentrated different morphological HA nanocrystals compared to the control sample. However, similar bacteria, treated with 2 mg/ml of HA samples, show no sharp decrease in catalase activity compared to the control. On treating both the bacteria with 0.2 mg/ml concentrated HA samples, their catalase activity increases when moving to HA nanorods to nanoplates and further to thin nanoplates. At 20 mg/ml, the catalase activity for both the bacteria significantly increases when the morphology changes from nanorods to nanoplates. However, it decreases when the morphology shifts from HA nanoplates to thin nanoplates. The overall analyses confirm that bacteria, cultured with HA nanorods (0.2 mg/ml) and HA thin nanoplates (20 mg/ml) possess significantly less catalase activity than control and other HA samples. The lower catalase activity is directly related to a slower rate of H_2O_2 dissociation, which means a larger number of toxic H_2O_2 within the bacterial cells, leading to less resistance towards bacterial death.

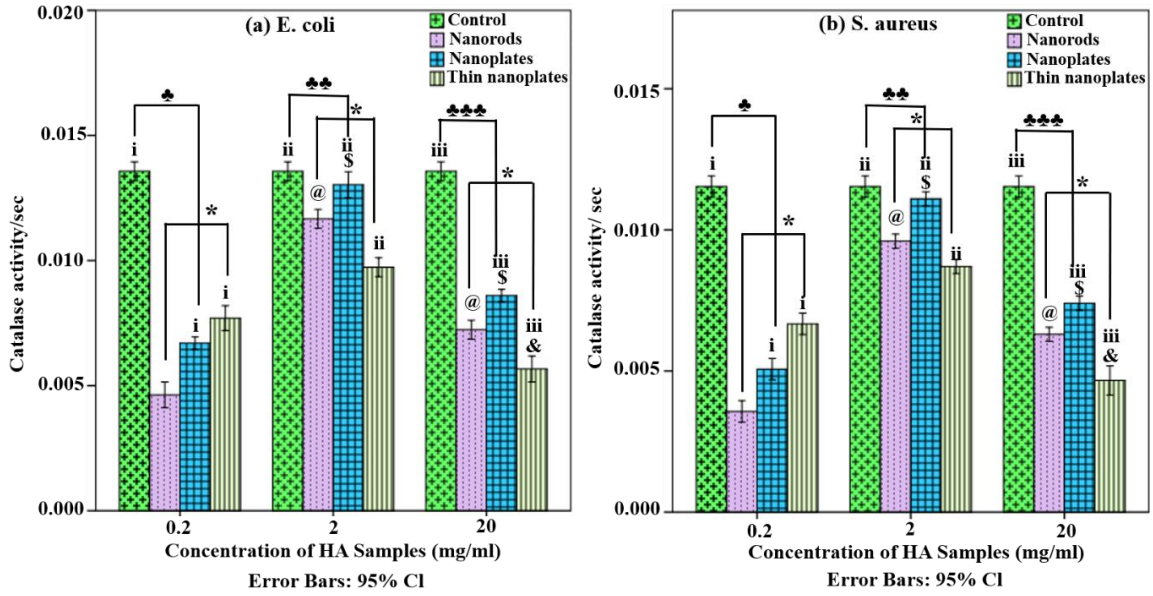

Figure 5.5. *The histogram plot representing catalase activity per second for evaluation of dissociated H_2O_2 of E. coli and S. aureus bacteria after treating with HA nanorods, nanoplates, and thin nanoplates at various concentrations of 0.2, 2 and 20 mg/ml. The mark (*) represents the significant difference in catalase activity for all the developed morphologies of HA nanocrystals at 0.2, 2 and 20 mg/ml with respect to control, at $p \leq 0.05$. The marks (i), (ii), and (iii) represent the significant difference in catalase activity of HA nanoplates and thin nanoplates as well as control as compared to HA nanorods at concentrations of 0.2, 2, and 20 mg/ml, respectively, at $p \leq 0.05$. The marks (♣), (♣♣), (♣♣♣) indicate the significant difference in catalase activity of HA nanorods and nanoplates as well as control as compared to HA thin nanoplates at concentrations of 0.2, 2, and 20 mg/ml, respectively, at $p \leq 0.05$. The marks (@), ($) and (&) show significant differences in the catalase activity of HA nanorods, nanoplates and thin nanoplates, respectively, with varying concentrations.*

5.1.3.3. ROS-induced damaged proteins

The overproduction of ROS damages intracellular components of bacteria, such as bacterial membrane, proteins, DNA and nucleic acid, which consequently leads to bacterial death. Therefore, the amount of intracellular damaged proteins is measured using Lowry method. Fig.

5.6 demonstrates histogram plots for the amount of ROS-induced damaged proteins of *E. coli* and *S. aureus* bacteria after treatment with HA nanorods, nanoplates, and thin nanoplates at varying concentrations of 0.2, 2 and 20 mg/ml. Statistical analyses reveal that both the bacteria, treated with 0.2 and 20 mg/ml concentration of HA nanocrystals, possess significantly higher quantities of damaged proteins than the control. At 0.2 mg/ml concentration, HA nanorods damage the highest amount of proteins of similar bacterial cells as compared to HA nanoplates and thin HA nanoplates. In contrast, at 20 mg/ml, HA thin nanoplates produce the highest amount of damaged protein as compared to HA nanorods and nanoplates. More specifically, the damaged proteins in 20 mg/ml of HA thin nanoplates are slightly lower as compared to 0.2 mg/ml of HA nanorods. It indicates the first highest production of ROS, i.e., $O^{2\bullet-}$ and H_2O_2 in the case of 0.2 mg/ml of HA nanorods and second in 20 mg/ml of HA thin nanoplates, as compared to control and other samples, which is well aligned with SOD and catalase results. It confirms that the amount of ROS production is directly proportional to oxidative damage within bacteria.

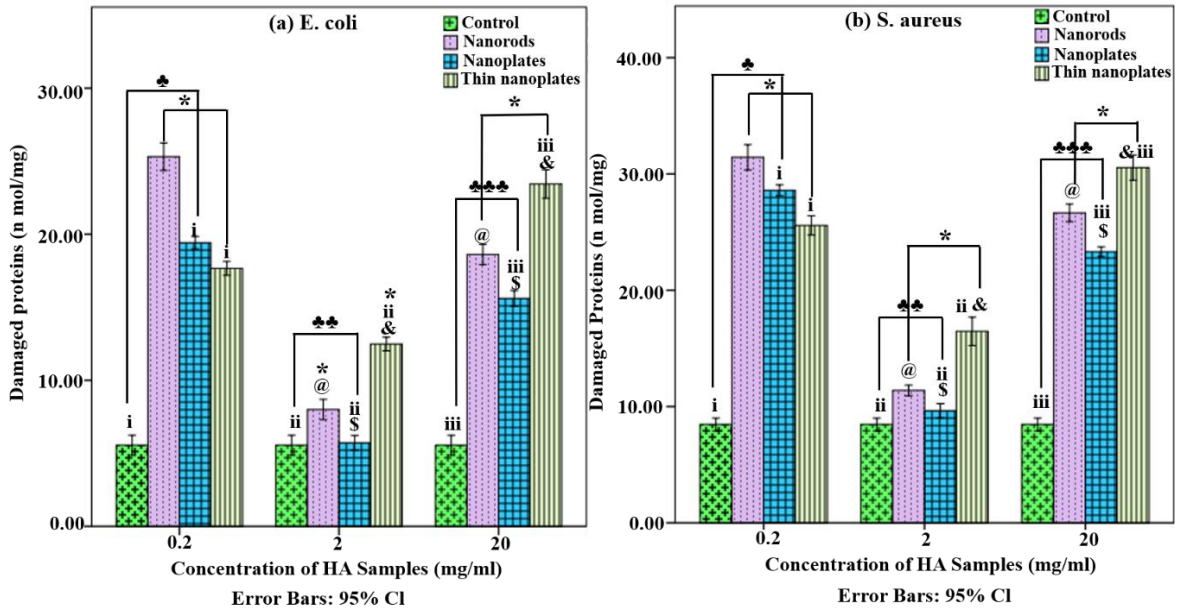

Figure 5.6. *Concentration of oxidative damaged proteins (n mol/mg) of E. coli (a) and S. aureus bacteria (b), after treated with HA nanorods, nanoplates, and thin nanoplates at various concentrations of 0.2, 2 and 20 mg/ml. The mark (*) represents the significant difference in concentration of damaged proteins for all morphologies of HA nanocrystals at 0.2, 2 and 20 mg/ml with respect to control, at $p \leq 0.05$. The marks (i), (ii) and (iii) represent the significant difference in concentration of damaged proteins of HA nanoplates and thin nanoplates as well as control, as compared to HA nanorods at concentrations of 0.2, 2, and 20 mg/ml at $p \leq 0.05$, respectively. The marks (♣), (♣♣), (♣♣♣) indicate the significant difference in concentration of leaked proteins of HA nanorods and nanoplates as well as control as compared to HA thin nanoplates at concentrations of 0.2, 2, and 20 mg/ml at $p \leq 0.05$, respectively. The marks (@), ($) and (&) show the significant difference in concentration of damaged proteins of HA nanorods, nanoplates and thin nanoplates, respectively, among the different concentrations.*

5.1.3.4. MDA estimation

The ROS-induced lipid damage of *E. coli* and *S. aureus* bacteria has been measured in terms of MDA formation. Fig. 5.7 represents the comparative assessment of MDA levels, formed in both the bacteria, when treated with different concentrations of HA nanocrystals (nanorods,

nanoplates, and thin nanoplates) as compared to the control material. 0.2 mg/ml concentrated HA nanocrystals produce the highest amount of MDA in HA nanorods, followed by HA nanoplates, and HA thin nanoplates. However, on increasing the concentration from 0.2 to 2 mg/ml, the MDA levels for all three morphologies sharply decreased to nearly MDA levels, as observed in control samples. On further increasing the concentration from 2 to 20 mg/ml, MDA levels increased again, with HA thin nanoplates showing the highest MDA, followed by HA nanorods and HA nanoplates. The results indicate that 0.2 mg/ml of HA nanorods and 20 mg/ml of HA thin nanoplates significantly promote LPO compared to the control and the rest of the samples, leading to corresponding lipid damage. These observations are also in good agreement with SOD and catalase results.

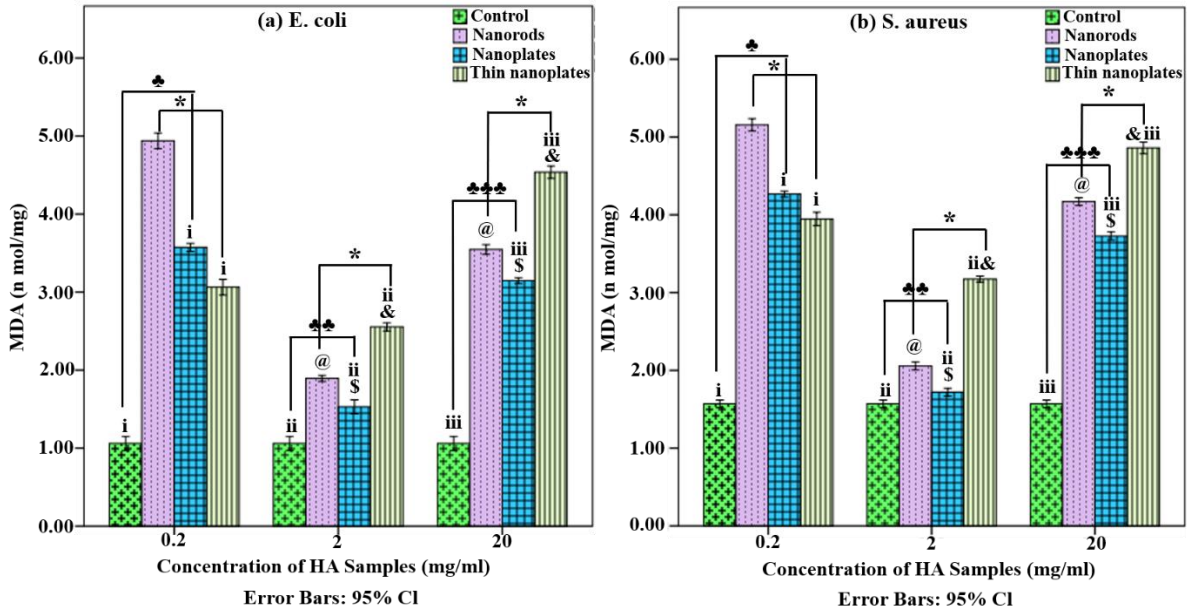

Figure 5.7. *Concentration of MDA (nmol/mg), produced on LPO of E. coli and S. aureus bacteria after treatment with HA nanorods, nanoplates, and thin nanoplates at various concentrations of 0.2, 2 and 20 mg/ml. The mark (*) represents the significant difference in concentration of MDA for all the developed morphologies of HA nanocrystals at 0.2, 2 and 20 mg/ml with respect to control, at $p \leq 0.05$. The marks (i), (ii), and (iii) represent the significant difference in concentration of MDA of HA nanoplates and thin nanoplates as well as control*

as compared to HA nanorods at concentrations of 0.2, 2, and 20 mg/ml, respectively, at $p \leq 0.05$. The marks (♣), (♣♣), (♣♣♣) indicate the significant difference in concentration of MDA of HA nanorods and nanoplates as well as control as compared to HA thin nanoplates at concentrations of 0.2, 2, and 20 mg/ml, respectively, $p \leq 0.05$. The marks (@), ($) and (&) show the significant difference in concentration of MDA of HA nanorods, nanoplates and thin nanoplates, respectively, among the different concentrations.

5.1.4. Mechanism for morphology-induced antibacterial response

Based on MTT results (Fig. 5.1), HA nanorods possess better antibacterial potential than HA nanoplates and thin nanoplates at a concentration of 0.2 mg/ml, which was further confirmed by qualitative tests, such as colony counting method (Fig. 5.2) and live-dead assay (Fig. 5.3). At 0.2 mg/ml, the higher concentration of ROS ($O_2^{\bullet-}$ and H_2O_2) is produced in HA nanorods as compared to HA nanoplates and thin nanoplates (Figs. 5.4 and 5.5). It allows corresponding oxidative damages in a similar manner for the above respective morphologies, as confirmed by ROS-induced protein leakage and MDA levels (Figs. 5.6 and 5.7). It clearly revealed that the overproduction of ROS is mainly responsible for the antibacterial activity of different morphological HA nanocrystals at 0.2 mg/ml. The difference in ROS generation among HA morphologies can be directly correlated to their size. The dimensions of HA nanorods and nanoplates are (70 – 500 × 22 – 62) nm^2 and (200 – 500 × 60 – 250 × 7 – 66) nm^3, respectively. However, the length of thin nanoplates is up to a micron scale with thickness down to ~7 nm. Clearly, a larger number of HA nanorods have a size of less than 100 nm, making them more susceptible to ROS generation due to their ease with cellular internalization and high surface area-to-volume ratio [28, 30, 69, 70]. Within bacteria, the electron donor sites of HA nanocrystals interact with molecular oxygen O_2 and convert to $O_2^{\bullet-}$ radical, which further generates toxic ROS, such as H_2O_2 and •OH [28, 29]. Smaller particles also promote ROS production by deactivating defense enzymes, and disturbing the electron-transfer process and

mitochondria function [71]. Therefore, HA nanorods have higher antibacterial activity at 0.2 mg/ml. However, the larger-sized HA nanoplates and thin nanoplates possess reduced antibacterial potential at this concentration.

At HA concentration of 2 mg/ml, the variation in antibacterial activity for HA nanorods, nanoplates, and thin nanoplates is in increasing order, differing from the trend observed at 0.2 mg/ml (Fig. 5.1). At this concentration, NPs internalization ceased due to their agglomeration and antibacterial effect primarily results from the combined action of Ca^{2+} ion release and electrostatic repulsion between HA nanocrystals and bacterial cells. In the cellular metabolic process, the Ca^{2+} ions increase the metabolic rate (ATP synthesis) of bacterial cells by activating the enzymes related to the Krebs cycle and oxidative phosphorylation in mitochondria, which would consume more molecular oxygen, resulting in enhanced ROS generation as a byproduct. This leads to oxidative stress and, ultimately, cell apoptosis [72, 73]. The release rate of Ca^{2+} ions is directly linked with the crystallinity of HA nanorods, nanoplates, and thin nanoplates, which is calculated to be ~ 89, 97 and 86 %, respectively. The lower crystallinity causes higher dissolution [74-76]. Consequently, at 2 mg/ml, ROS production and their associated bacterial damage are the highest in HA thin nanoplates and the lowest in HA nanoplates (Figs. 5.4, 5.5, 5.6 and 5.7), resulting in minimum antibacterial activity for HA nanoplates as compared to HA nanorods and thin nanoplates. In contrast, both quantitative and qualitative tests revealed the least antibacterial activity for HA nanorods than HA nanoplates and thin nanoplates at 2 mg/ml (Figs, 5.1, 5.2 and 5.3). Apart from achieving the antibacterial response of HA nanocrystals (2 mg/ml) due to oxidative stress, generated by the release of Ca^{2+} ions, the electrostatic repulsion between HA nanocrystals and bacterial cells also contributes significantly to further enhance the antibacterial activity of HA nanoplates and thin nanoplates [77, 78].

It is well reported that hexagonal HA possess two oppositely charged crystal planes; positively charged a-plane (rich in Ca^{2+} ions) and negatively charged c-plane (enriched with PO_4^{3-} and OH^- ions) [79-81]. Since both, *E. coli* and *S. aureus* bacteria possess a negative charge [82], at 2 mg/ml, bacterial adhesion is lower in HA nanoplates and thin nanoplates, as their major exposed surface of interaction with bacterial cells is along the negatively charged c-plane [Fig. 3.9C (b3 and c3)]. However, the major exposed surface of HA nanorods for interaction with bacterial cells is along the positively charged a (b)-plane [(Fig. 3.9C (a3)], leading to more bacterial adhesions (Fig. 5.2 and 5.3). Several studies also observed a high number of adherent *E. coli* and *S. aureus* bacteria on positively charged surfaces [83]. The antibacterial activity of HA nanorods is only due to ROS production from Ca^{2+} ions release. While HA nanoplates and thin nanoplates showed antibacterial activity due to both, Ca^{2+} ions release and electrostatic repulsion. As a result, HA nanorods show the lowest antibacterial activity compared to HA nanoplates and thin nanoplates at 2 mg/ml (Fig. 5.1, 5.2, and 5.3). On further increasing the concentration of HA nanocrystals from 2 – 20 mg/ml, a similar variation for HA nanorods, nanoplates, and thin nanoplates is observed (Fig. 5.1). Even their antibacterial activity is significantly enhanced for both, *E. coli* and *S. aureus* bacteria. Treating the bacteria with increased HA concentration enhances the number of released Ca^{2+} ions and the degree of repulsion between HA nanocrystals and bacterial cells [84, 85].

It can, therefore, be suggested that the antibacterial activity of HA nanocrystals is morphology and dose-dependent.

5.2. Summary

In this chapter, antibacterial activity of various concentrations (0.2, 2 and 20 mg/ml) and morphologies of HA nanocrystals were evaluated using a number of quantitative and qualitative assays. The results revealed that HA nanorods and thin nanoplates exhibited good antibacterial response at concentrations of 0.2 and 20 mg/ml, respectively. Even 20 mg/ml

concentrated HA thin nanoplates showed the highest antibacterial response among all the tested concentrations and other samples. Moreover, the least antibacterial response was observed for HA nanorods at the concentration of 2 mg/ ml. The mechanism for the bactericidal effect of HA nanocrystals was also revealed by SOD, catalase, protein estimation and lipid peroxidation assays. The bactericidal effect of 0.2 mg/ml concentrated HA nanorods was due to over production of ROS within the bacterial cells. In contrast, 20 mg/ml concentrated thin HA nanoplates showed antibacterial potential due to the synergistic effect of ROS generation and their electrostatic repulsion with bacteria. It can, therefore, be suggested that HA thin nanoplates can be a potential antibacterial biomaterial to prevent prosthetic implant-related bacterial infection (Fig. 5.8).

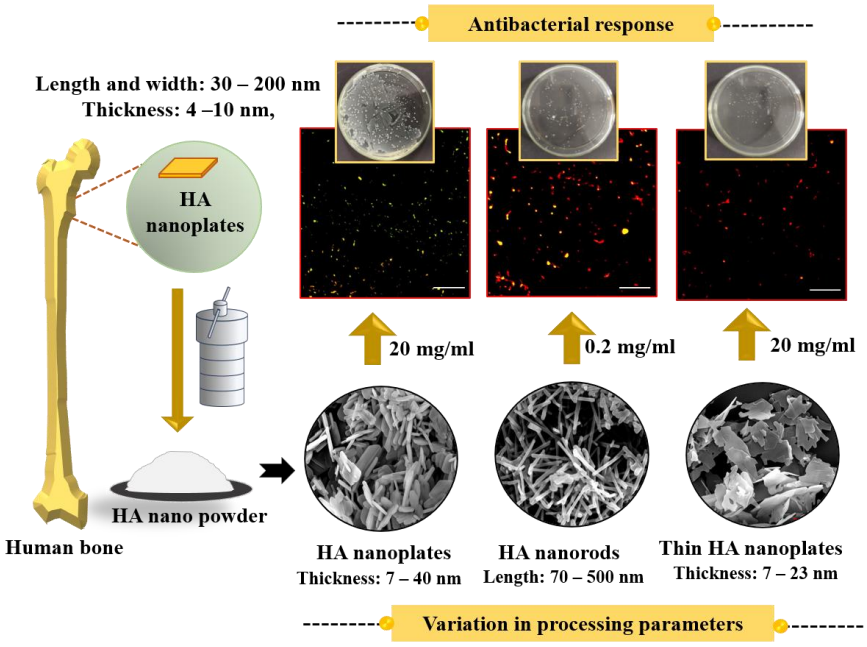

Fig. 5.8 *Schematic diagram, demonstrating the antibacterial efficacy of different morphological HA nanocrystals*

References

[1] P. Shree, C.K. Singh, K.K. Sodhi, J.N. Surya, D.K. Singh, Biofilms: Understanding the structure and contribution towards bacterial resistance in antibiotics, Medicine in Microecology 16 (2023) 100084.

[2] Y. Lu, W.J. Cai, The Role of Staphylococcal Biofilm on the Surface of Implants in Orthopedic Infection, 10(10) (2022).

[3] L. Crémet, S. Corvec, P. Bémer, L. Bret, C. Lebrun, B. Lesimple, A.-F. Miegeville, A. Reynaud, D. Lepelletier, N. Caroff, Orthopaedic-implant infections by Escherichia coli: Molecular and phenotypic analysis of the causative strains, Journal of Infection 64(2) (2012) 169-175.

[4] Y. Min, S. Wu, W. Li, Y. Ma, Y. Wang, P. Zhang, Y. Zheng, One-pot synthesis of multipod Au-Cu nanocrystals with tunable branching for efficient photothermal treatment against multidrug-resistant bacteria, Journal of Alloys and Compounds 976 (2024) 172935.

[5] A. Singh, A.K. Dubey, Various Biomaterials and Techniques for Improving Antibacterial Response, ACS Applied Bio Materials 1(1) (2018) 3-20.

[6] F.D. Al-Shalawi, A.H. Mohamed Ariff, D.-W. Jung, M.K. Mohd Ariffin, C.L. Seng Kim, D. Brabazon, M.O. Al-Osaimi, Biomaterials as Implants in the Orthopedic Field for Regenerative Medicine: Metal versus Synthetic Polymers, Polymers, 2023.

[7] B.L. Smith, S. Fernando, M.D. King, Escherichia coli resistance mechanism AcrAB-TolC efflux pump interactions with commonly used antibiotics: a molecular dynamics study, Scientific Reports 14(1) (2024) 2742.

[8] W.C. Reygaert, An overview of the antimicrobial resistance mechanisms of bacteria, AIMS microbiology 4(3) (2018) 482-501.

[9] J.P. Coleman, C.J. Smith, Microbial Resistance☆, Reference Module in Biomedical Sciences, Elsevier2014.

[10] L. Wang, C. Hu, L. Shao, The antimicrobial activity of nanoparticles: present situation and prospects for the future, International journal of nanomedicine 12 (2017) 1227-1249.

[11] K. Baskar, T. Anusuya, G. Devanand Venkatasubbu, Mechanistic investigation on microbial toxicity of nano hydroxyapatite on implant associated pathogens, Materials science & engineering. C, Materials for biological applications 73 (2017) 8-14.

[12] A. S, H.P. Kavitha, Magnesium Oxide Nanoparticles: Effective Antilarvicidal and Antibacterial Agents, ACS Omega 8(6) (2023) 5225-5233.

[13] M. Azizi-Lalabadi, A. Ehsani, B. Divband, M. Alizadeh-Sani, Antimicrobial activity of Titanium dioxide and Zinc oxide nanoparticles supported in 4A zeolite and evaluation the morphological characteristic, Scientific Reports 9(1) (2019) 17439.

[14] O.B. Ahmed, T. Alamro, Evaluation of the antibacterial activities of face masks coated with titanium dioxide nanoparticles, Scientific Reports 12(1) (2022) 18739.

[15] M.A. Ansari, H.M. Khan, A.A. Khan, R. Pal, S.S. Cameotra, Antibacterial potential of Al2O3 nanoparticles against multidrug resistance strains of Staphylococcusaureus isolated from skin exudates, Journal of Nanoparticle Research 15(10) (2013) 1970.

[16] L. Gabrielyan, A. Hovhannisyan, V. Gevorgyan, M. Ananyan, A. Trchounian, Antibacterial effects of iron oxide (Fe3O4) nanoparticles: distinguishing concentration-dependent effects with different bacterial cells growth and membrane-associated mechanisms, Applied Microbiology and Biotechnology 103(6) (2019) 2773-2782.

[17] D. Laha, A. Pramanik, A. Laskar, M. Jana, P. Pramanik, P. Karmakar, Shape-dependent bactericidal activity of copper oxide nanoparticle mediated by DNA and membrane damage, Materials Research Bulletin 59 (2014) 185-191.

[18] G.S. Kumar, S. Rajendran, S. Karthi, R. Govindan, E.K. Girija, G. Karunakaran, D. Kuznetsov, Green synthesis and antibacterial activity of hydroxyapatite nanorods for orthopedic applications, MRS Communications 7(2) (2017) 183-188.

[19] H. Abed, N. H, E. Salim, Influence of nano-hydroxyapatite particles on the mechanical and antibacterial properties of polycarbonate films, Materials Research Express 10 (2023).

[20] N. Talebian, S.M. Amininezhad, M. Doudi, Controllable synthesis of ZnO nanoparticles and their morphology-dependent antibacterial and optical properties, Journal of Photochemistry and Photobiology B: Biology 120 (2013) 66-73.

[21] X. Hong, J. Wen, X. Xiong, Y. Hu, Shape effect on the antibacterial activity of silver nanoparticles synthesized via a microwave-assisted method, Environmental science and pollution research international 23(5) (2016) 4489-97.

[22] T.C. Dakal, A. Kumar, R.S. Majumdar, V. Yadav, Mechanistic Basis of Antimicrobial Actions of Silver Nanoparticles, Frontiers in microbiology 7 (2016) 1831.

[23] D.L. Slomberg, Y. Lu, A.D. Broadnax, R.A. Hunter, A.W. Carpenter, M.H. Schoenfisch, Role of Size and Shape on Biofilm Eradication for Nitric Oxide-Releasing Silica Nanoparticles, ACS Applied Materials & Interfaces 5(19) (2013) 9322-9329.

[24] T. Yao, J. Chen, Z. Wang, J. Zhai, Y. Li, J. Xing, S. Hu, G. Tan, S. Qi, Y. Chang, P. Yu, C. Ning, The antibacterial effect of potassium-sodium niobate ceramics based on controlling piezoelectric properties, Colloids and Surfaces B: Biointerfaces 175 (2019) 463-468.

[25] S.J. Kim, H.S. Kim, Y.R. Seo, Understanding of ROS-Inducing Strategy in Anticancer Therapy, Oxidative Medicine and Cellular Longevity 2019(1) (2019) 5381692.

[26] A.V. Samrot, S.P. Ram Singh, R. Deenadhayalan, V.V. Rajesh, S. Padmanaban, K. Radhakrishnan, Nanoparticles, a Double-Edged Sword with Oxidant as Well as Antioxidant Properties—A Review, Oxygen, 2022, pp. 591-604.

[27] L. Han, Q. He, Y. Wang, X. Chen, H. Sun, Y. Ma, Y. Wang, P. Zhang, X. Wu, Y. Zheng, Synergistic antibacterial effects of selenium-doped gold nanosheets with notable near infrared-II photothermal conversion against multidrug-resistant bacteria, Colloids and Surfaces A: Physicochemical and Engineering Aspects 703 (2024) 135394.

[28] A. Nel, T. Xia, L. Mädler, N. Li, Toxic potential of materials at the nanolevel, Science (New York, N.Y.) 311(5761) (2006) 622-7.

[29] A. Manke, L. Wang, Y. Rojanasakul, Mechanisms of nanoparticle-induced oxidative stress and toxicity, BioMed research international 2013 (2013) 942916.

[30] P.P. Fu, Q. Xia, H.M. Hwang, P.C. Ray, H. Yu, Mechanisms of nanotoxicity: generation of reactive oxygen species, Journal of food and drug analysis 22(1) (2014) 64-75.

[31] K. Keyer, A.S. Gort, J.A. Imlay, Superoxide and the production of oxidative DNA damage, Journal of bacteriology 177(23) (1995) 6782-90.

[32] N. Khare, D. Goyary, N.K. Singh, P. Shah, M. Rathore, S. Anandhan, D. Sharma, M. Arif, Z. Ahmed, Transgenic tomato cv. Pusa Uphar expressing a bacterial mannitol-1-phosphate dehydrogenase gene confers abiotic stress tolerance, Plant Cell, Tissue and Organ Culture (PCTOC) 103(2) (2010) 267-277.

[33] H. Aebi, [13] Catalase in vitro, Methods in Enzymology, Academic Press1984, pp. 121-126.

[34] O. Lowry, N. Rosebrough, A.L. Farr, R. Randall, PROTEIN MEASUREMENT WITH THE FOLIN PHENOL REAGENT, Journal of Biological Chemistry 193(1) (1951) 265-275.

[35] C.M. Pomory, Color development time of the Lowry protein assay, Analytical Biochemistry 378(2) (2008) 216-217.

[36] A.C. Gasparovic, M. Jaganjac, B. Mihaljevic, S.B. Sunjic, N. Zarkovic, Assays for the Measurement of Lipid Peroxidation, in: L. Galluzzi, I. Vitale, O. Kepp, G. Kroemer (Eds.), Cell Senescence: Methods and Protocols, Humana Press, Totowa, NJ, 2013, pp. 283-296.

[37] A. Ayala, M.F. Muñoz, S. Argüelles, Lipid peroxidation: production, metabolism, and signaling mechanisms of malondialdehyde and 4-hydroxy-2-nonenal, Oxid Med Cell Longev 2014 (2014) 360438.

[38] G.A. Martínez-Castañón, J.P. Loyola-Rodríguez, N.V. Zavala-Alonso, S.E. Hernández-Martínez, N. Niño-Martínez, G. Ortega-Zarzosa, F. Ruiz, Preparation and characterization of nanostructured powders of hydroxyapatite, Superficies y vacío 25(2) (2012) 101-105.

[39] H. Kim, R.P. Camata, Y.K. Vohra, W.R. Lacefield, Control of phase composition in hydroxyapatite/tetracalcium phosphate biphasic thin coatings for biomedical applications, Journal of Materials Science: Materials in Medicine 16(10) (2005) 961-966.

[40] W. Liang, Y. Niu, S. Ge, S. Song, J. Su, Z. Luo, Effects of hydrothermal treatment on the properties of nanoapatite crystals, International journal of nanomedicine 7 (2012) 5151-8.

[41] J.S. Cho, S.-H. Rhee, Formation mechanism of nano-sized hydroxyapatite powders through spray pyrolysis of a calcium phosphate solution containing polyethylene glycol, Journal of the European Ceramic Society 33(2) (2013) 233-241.

[42] D. Kong, X. Xiao, X. Qiu, W. Zhang, Y. Yang, Synthesis of Hydroxyapatite Nanorods under Mild Conditions and Their Drug Release Properties, Chinese Journal of Chemistry 33(9) (2015) 1024-1030.

[43] A.J. Nathanael, Y.H. Seo, T.H. Oh, PVP Assisted Synthesis of Hydroxyapatite Nanorods with Tunable Aspect Ratio and Bioactivity, Journal of Nanomaterials 2015 (2015) 621785.

[44] G. Bharath, A. Jagadeesh Kumar, K. Karthick, D. Mangalaraj, C. Viswanathan, N. Ponpandian, Shape evolution and size controlled synthesis of mesoporous hydroxyapatite nanostructures and their morphology dependent Pb(ii) removal from waste water, RSC Advances 4(70) (2014) 37446-37457.

[45] R.R. Kimaka P, P. Wang, M. He, S. Meng, J. Yao, H. Li, C. Yang, Z. Li, Ce- and La-doped polymetallic layered double hydroxides for enhanced oxygen evolution reaction performance at high current density, Science China Chemistry 67(8) (2024) 2586-2598.

[46] H. Esfahani, E. Salahi, A. Tayebifard, M.R. Rahimipour, M. Keyanpour-Rad, Influence of zinc incorporation on microstructure of hydroxyapatite to characterize the effect of pH and calcination temperatures, Journal of Asian Ceramic Societies 2(3) (2014) 248-252.

[47] Y. In, U. Amornkitbamrung, M.-H. Hong, H. Shin, On the Crystallization of Hydroxyapatite under Hydrothermal Conditions: Role of Sebacic Acid as an Additive, ACS Omega 5(42) (2020) 27204-27210.

[48] F. Ren, Y. Ding, Y. Leng, Infrared spectroscopic characterization of carbonated apatite: A combined experimental and computational study, Journal of Biomedical Materials Research Part A 102(2) (2014) 496-505.

[49] E.A. Taylor, C.J. Mileti, S. Ganesan, J.H. Kim, E. Donnelly, Measures of Bone Mineral Carbonate Content and Mineral Maturity/Crystallinity for FT-IR and Raman Spectroscopic Imaging Differentially Relate to Physical–Chemical Properties of Carbonate-Substituted Hydroxyapatite, Calcified Tissue International 109(1) (2021) 77-91.

[50] A.A. Bonapasta, F. Buda, P. Colombet, G. Guerrini, Cross-Linking of Poly(Vinyl Alcohol) Chains by Ca Ions in Macro-Defect-Free Cements, Chemistry of Materials 14(3) (2002) 1016-1022.

[51] D. Jahani, A. Nazari, J. Ghourbanpour, A. Ameli, Polyvinyl Alcohol/Calcium Carbonate Nanocomposites as Efficient and Cost-Effective Cationic Dye Adsorbents, Polymers, 2020.

[52] Y. Bao, X. Huang, J. Xu, S. Cui, Effect of Intramolecular Hydrogen Bonds on the Single-Chain Elasticity of Poly(vinyl alcohol): Evidencing the Synergistic Enhancement Effect at the Single-Molecule Level, Macromolecules 54(15) (2021) 7314-7320.

[53] K. Suchanek, A. Bartkowiak, M. Perzanowski, M. Marszałek, From monetite plate to hydroxyapatite nanofibers by monoethanolamine assisted hydrothermal approach, Scientific Reports 8(1) (2018) 15408.

[54] H. Maeda, T. Kawai, S. Sekii, Intra- and intermolecular hydrogen bonds in polyvinyl alcohol solutions, Journal of Polymer Science 35(128) (1959) 288-292.

[55] M.J. Nugent, A. Hanley, P.T. Tomkins, C.L. Higginbotham, Investigation of a novel freeze-thaw process for the production of drug delivery hydrogels, Journal of materials science. Materials in medicine 16(12) (2005) 1149-58.

[56] M.A. Darabi, A. Khosrozadeh, Y. Wang, N. Ashammakhi, H. Alem, A. Erdem, Q. Chang, K. Xu, Y. Liu, G. Luo, A. Khademhosseini, M. Xing, An Alkaline Based Method for Generating Crystalline, Strong, and Shape Memory Polyvinyl Alcohol Biomaterials, Advanced Science 7(21) (2020) 1902740.

[57] C. Zhang, J. Yang, Z. Quan, P. Yang, C. Li, Z. Hou, J. Lin, Hydroxyapatite Nano- and Microcrystals with Multiform Morphologies: Controllable Synthesis and Luminescence Properties, Crystal Growth & Design 9(6) (2009) 2725-2733.

[58] X. Wang, L. Zhang, Z. Liu, Q. Zeng, G. Jiang, M. Yang, Probing the surface structure of hydroxyapatite through its interaction with hydroxyl: a first-principles study, RSC Advances 8(7) (2018) 3716-3722.

[59] D.-J. Wu, Z.-X. Liu, C.-Z. Gao, X.-C. Shen, X.-M. Wang, H. Liang, Effect of methyl and hydroxyl functional group surfaces on crystallization of hydroxyapatite coating, Surface and Coatings Technology 228 (2013) S24-S27.

[60] N. Thanh, N. Maclean, S. Mahiddine, Mechanisms of Nucleation and Growth of Nanoparticles in Solution, Chemical Reviews 114 (2014).

[61] Z. Ecsedi, I. Lazău, C. Păcurariu, Synthesis of mesoporous alumina using polyvinyl alcohol template as porosity control additive, Processing and Application of Ceramics 1 (2007).

[62] G. Zuo, X. Wei, H. Sun, S. Liu, P. Zong, X. Zeng, Y. Shen, Morphology controlled synthesis of nano-hydroxyapatite using polyethylene glycol as a template, Journal of Alloys and Compounds 692 (2017) 693-697.

[63] F. Ren, Y. Ding, X. Ge, X. Lu, K. Wang, Y. Leng, Growth of one-dimensional single-crystalline hydroxyapatite nanorods, Journal of Crystal Growth 349(1) (2012) 75-82.

[64] P. Wang, S. Meng, B. Zhang, M. He, P. Li, C. Yang, G. Li, Z. Li, Sub-1 nm Cu2O Nanosheets for the Electrochemical CO2 Reduction and Valence State–Activity Relationship, Journal of the American Chemical Society 145(48) (2023) 26133-26143.

[65] M. Jevtić, M. Mitrić, S. Škapin, B. Jančar, N. Ignjatović, D. Uskoković, Crystal Structure of Hydroxyapatite Nanorods Synthesized by Sonochemical Homogeneous Precipitation, Crystal Growth & Design 8(7) (2008) 2217-2222.

[66] A.J. Nathanael, S.I. Hong, T.H. Oh, Y.H. Seo, D. Singh, S.S. Han, Enhanced cell viability of hydroxyapatite nanowires by surfactant mediated synthesis and its growth mechanism, RSC Advances 6(30) (2016) 25070-25081.

[67] Y. Wen, J. Liu, F. Zhang, Z. Li, P. Wang, Z. Fang, M. He, J. Chen, W. Song, R. Si, L. Wang, Mesoporous MnO2 nanosheets for efficient electrocatalytic nitrogen reduction via high spin polarization induced by oxygen vacancy, Nano Research 16(4) (2023) 4664-4670.

[68] F. Collin, Chemical Basis of Reactive Oxygen Species Reactivity and Involvement in Neurodegenerative Diseases, International journal of molecular sciences 20(10) (2019).

[69] B. Sadeghi, F.S. Garmaroudi, M. Hashemi, H.R. Nezhad, A. Nasrollahi, S. Ardalan, S. Ardalan, Comparison of the anti-bacterial activity on the nanosilver shapes: Nanoparticles, nanorods and nanoplates, Advanced Powder Technology 23(1) (2012) 22-26.

[70] D. Khare, A. Singh, A.K. Dubey, Influence of Na and K contents on the antibacterial response of piezoelectric biocompatible NaxK1-xNbO3 (x = 0.2–0.8), Materials Today Communications 27 (2021) 102317.

[71] Z. Yu, Q. Li, J. Wang, Y. Yu, Y. Wang, Q. Zhou, Reactive Oxygen Species-Related Nanoparticle Toxicity in the Biomedical Field, 15(1) (2020) 115.

[72] P.S. Brookes, Y. Yoon, J.L. Robotham, M.W. Anders, S.S. Sheu, Calcium, ATP, and ROS: a mitochondrial love-hate triangle, American journal of physiology. Cell physiology 287(4) (2004) C817-33.

[73] A. Görlach, K. Bertram, S. Hudecova, O. Krizanova, Calcium and ROS: A mutual interplay, Redox Biology 6 (2015) 260-271.

[74] W. Xue, X. Liu, X. Zheng, C. Ding, Effect of hydroxyapatite coating crystallinity on dissolution and osseointegration in vivo, Journal of Biomedical Materials Research Part A 74A(4) (2005) 553-561.

[75] Y. Li, Y. Wang, Y. Li, W. Luo, J. Jiang, J. Zhao, C. Liu, Controllable Synthesis of Biomimetic Hydroxyapatite Nanorods with High Osteogenic Bioactivity, ACS Biomaterials Science & Engineering 6(1) (2020) 320-328.

[76] H.S. Purohit, G.G.Z. Zhang, Y. Gao, Detecting Crystallinity in Amorphous Solid Dispersions Using Dissolution Testing: Considerations on Properties of Drug Substance, Drug Product, and Selection of Dissolution Media, Journal of Pharmaceutical Sciences 112(1) (2023) 290-303.

[77] G. Hwang, I.-S. Ahn, B.J. Mhin, J.-Y. Kim, Adhesion of nano-sized particles to the surface of bacteria: Mechanistic study with the extended DLVO theory, Colloids and Surfaces B: Biointerfaces 97 (2012) 138-144.

[78] A.P.V. Ferreyra Maillard, J.C. Espeche, P. Maturana, A.C. Cutro, A. Hollmann, Zeta potential beyond materials science: Applications to bacterial systems and to the development of novel antimicrobials, Biochimica et Biophysica Acta (BBA) - Biomembranes 1863(6) (2021) 183597.

[79] J.-J. Guan, B. Tian, S. Tang, Q.-F. Ke, C.-Q. Zhang, Z.-A. Zhu, Y.-P. Guo, Hydroxyapatite coatings with oriented nanoplate arrays: synthesis, formation mechanism and cytocompatibility, Journal of Materials Chemistry B 3(8) (2015) 1655-1666.

[80] Z. Zhuang, H. Yoshimura, M. Aizawa, Synthesis and ultrastructure of plate-like apatite single crystals as a model for tooth enamel, Materials Science and Engineering: C 33(5) (2013) 2534-2540.

[81] Z. Zhuang, H. Yamamoto, M. Aizawa, Synthesis of plate-shaped hydroxyapatite via an enzyme reaction of urea with urease and its characterization, Powder Technology 222 (2012) 193-200.

[82] P. Singh, A.K. Dubey, Electret-induced antibacterial response of Mg1-CaSi1-ZrO3 (x = 0–0.4) bioceramics, Journal of the American Ceramic Society 107(6) (2024) 4263-4281.

[83] G. Harkes, J. Feijen, J. Dankert, Adhesion of Escherichia coli on to a series of poly(methacrylates) differing in charge and hydrophobicity, Biomaterials 12(9) (1991) 853-60.

[84] L.A. Tamayo, P.A. Zapata, N.D. Vejar, M.I. Azócar, M.A. Gulppi, X. Zhou, G.E. Thompson, F.M. Rabagliati, M.A. Páez, Release of silver and copper nanoparticles from polyethylene nanocomposites and their penetration into Listeria monocytogenes, Materials Science and Engineering: C 40 (2014) 24-31.

[85] Y.N. Slavin, J. Asnis, U.O. Häfeli, H. Bach, Metal nanoparticles: understanding the mechanisms behind antibacterial activity, Journal of Nanobiotechnology 15(1) (2017) 65.